Q. J. R. Meteorol. Soc. (2004), **130**, pp. 2891–2918 doi: 10.1256/qj.03.187

Reflectivity and rain rate in and below drizzling stratocumulus

By KIMBERLY K. COMSTOCK*, ROBERT WOOD, SANDRA E. YUTER and CHRISTOPHER S. BRETHERTON

Department of Atmospheric Sciences, University of Washington, USA

(Received 29 September 2003; revised 6 July 2004)

SUMMARY

Ship-based radar measurements obtained during the East Pacific Investigation of Climate 2001 stratocumulus (Sc) cruise are used to derive characteristics of the rainfall from drizzling Sc. Reflectivity to rain rate (Z–R) relationships are determined from shipboard raindrop-size distribution measurements obtained from observations using filter-paper, and compared to Z–R relationships derived from aircraft probe data from below north-east Atlantic drizzling Sc and stratus. A model for the evaporation and sedimentation of drizzle is combined with reflectivity profiles from a millimetre-wavelength cloud radar to derive information on the mean raindrop radius and drizzle drop concentrations at cloud base, and to show how Z–R relationships change with height below the cloud base. The Z–R relationships are used in conjunction with shipborne C-band radar reflectivity data to estimate areal average precipitation with uncertainties at cloud base and at the surface. In the Sc drizzle Z–R relationship, $Z = aR^b$ (where a and b are constants), the estimated exponent $b = 1.1$ to 1.4 is lower than commonly observed in deep convective rain ($b = 1.5$). Analyses indicate that variations in Sc rain rates and reflectivities are influenced both by fluctuations in drizzle drop concentration and in mean radius, but that number concentration contributes more to the modulation of rain rate in Sc. Rain rates derived using the scanning C-band radar are found to be spatially variable, with much of the accumulation originating from a small fraction of the drizzling area. The observations also suggest that rain rate in marine Sc is strongly dependent on cloud liquid-water path, and inversely correlated with cloud droplet concentration.

KEYWORDS: Drizzle Drop-size distribution Marine boundary layer Stratus Z–R relationship

1. INTRODUCTION

Stratocumulus (Sc) clouds play an integral role in the earth's climate system. Large regions of Sc exist off the west coast of continents in the subtropics (Klein and Hartmann 1993). The low, warm Sc clouds reflect a substantial amount of incoming solar radiation but have only a small effect on the net outgoing long-wave radiation compared to the sea surface. The substantial areal extent and persistence of Sc clouds make them important to global climate (e.g. Slingo 1990). Philander *et al.* (1996) found that the presence of low-level stratus was also crucial to the positioning of the Pacific intertropical convergence zone north of the equator. Sc drizzle is associated with latent heating in the clouds, and is a primary means of removing water from the marine boundary layer (MBL) that could otherwise condense into cloud. A portion of the drizzle evaporates; this cools the sub-cloud layer, stabilizes the MBL against turbulence, and could potentially decouple the cloud layer (e.g. Turton and Nicholls 1987). Significant below-cloud evaporation was observed at times during the second Lagrangian experiment in the Atlantic Sc Transition Experiment (ASTEX; Bretherton *et al.* 1995), but few of the studies focusing on Sc have examined the evaporation of drizzle. In this paper, we estimate drizzle both at cloud base and at the surface using ship-based radar observations. This dataset from EPIC (Eastern Pacific Investigation of Climate 2001) Sc provides an unprecedented opportunity to quantify the mean characteristics and spatio–temporal variability of drizzle, and its relation to MBL and cloud characteristics in a subtropical stratocumulus regime.

The EPIC Sc cruise in October 2001 (Bretherton *et al.* 2004) was an extensive examination of the Sc region near Peru (20°S, 85°W). As in the TEPPS Sc cruise (Yuter *et al.* 2000) off the coast of Mexico, EPIC Sc used a scanning C-band radar

* Corresponding author: Department of Atmospheric Sciences, University of Washington, Box 351640, Seattle, WA 98195, USA. e-mail: kcomstock@atmos.washington.edu

aboard the National Oceanic and Atmospheric Administration (NOAA) ship the *Ronald H. Brown* (RHB) to obtain areal information on the structure of the drizzling Sc. During EPIC Sc, the RHB was also equipped with a NOAA Environmental Technology Laboratory (ETL) vertically pointing millimetre-wavelength cloud radar (MMCR), a microwave radiometer, and a suite of other instruments for sampling the ocean and atmospheric boundary layer. We use the C-band radar data from EPIC Sc in conjunction with a derived relationship between radar reflectivity (Z) and rain rate (R) to obtain areal average drizzle statistics. MMCR data are used to examine below-cloud evaporation of drizzle. The radar data used in this study are unique, because of the ship's location within the south-east Pacific Sc region, the sample duration of several days and the large area sampled by the scanning radar.

Previous field studies of drizzling Sc have used aircraft radar and *in situ* data to estimate rain rates along and near the flight track (e.g. Austin *et al.* 1995; Vali *et al.* 1998; Stevens *et al.* 2003), and surface-based vertically pointing radar to obtain profiles of precipitation characteristics (e.g. Miller and Albrecht 1995). Because no *in situ* cloud data were available for this campaign, data obtained on 12 flights in the north-east Atlantic between 1990 and 2000 aboard the UK Met Office C-130 aircraft (Wood 2005) are used for verification and comparison of our techniques and results.

The data used in our analysis are described in section 2, and the procedure for obtaining Z–R relationships is outlined in section 3. Section 3 also includes an examination of below-cloud evaporation of drizzle using an evaporation–sedimentation model. In section 4 the effect of evaporation on the parameters in the Z–R relationships is discussed. Also in section 4, reflectivity and rain rate are each expressed as functions of drizzle drop number concentration and mean size, and these are used as additional means to estimate the exponent b in the Z–R relationship, $Z = aR^b$, where a and b are constants. We show that all of our datasets and methods yield similar Z–R relationships for Sc drizzle. In section 5, the Z–R relations are applied to EPIC and TEPPS C-band radar data to estimate rainfall amounts, their probability distribution at cloud base, and the quantity of rainfall reaching the surface. We also determine an empirical relationship among rain rate, liquid-water path, and droplet concentration that will be useful in the development of model parametrizations of drizzle.

2. Data

(*a*) *Filter-paper data samples*

Filter-paper treated with a water-sensitive dye (methylene blue, or 'meth blue') is a time-tested, but labour-intensive technique for observing rain drop-size distributions (DSDs). Filter-paper DSD samples were taken aboard the RHB because ship vibrations interfere with disdrometer measurements and the ship's rain-gauges were not sensitive to small amounts of drizzle (Yuter and Parker 2001). During EPIC Sc, the 23.8 cm diameter filter-paper was exposed to precipitation for a timed duration (up to 2 minutes), and the drops were counted and categorized by hand into eight evenly spaced bins between 0.1 and 0.8 mm radius, establishing a DSD for each sample. The preparation and collection of filter-paper samples is described by Rinehart (1997). The range of resolvable drop sizes is assumed to be sufficient to determine a Z–R relationship. The minimum detectable drop size is 0.1 mm radius. During the EPIC Sc cruise, 33 samples were collected during 23 separate drizzle episodes. When possible, two samples were collected in sequence to check the consistency of the DSD. Six filter-paper samples were also analysed from the TEPPS Sc cruise.

(*b*) *Samples from aircraft in situ microphysics*

Aircraft DSD data were collected on 12 flights in and below drizzling Sc clouds off the coast of the UK. The UK Met Office C-130 aircraft was equipped with a Particle Measuring Systems (PMS) Inc. Forward Scattering Spectrometer Probe, which counted cloud drops between 1 and 23.5 μm radius and categorized them in 15 evenly spaced bins. The PMS 2D-C optical array probe counted drops in 32 size categories between 12.5 and 400 μm radius. Post-processing by linear interpolation produced combined DSDs from the two instruments (Wood 2005). On constant-height in-cloud flights, samples were averaged over about 10 minutes, corresponding to 50–100 km; on 'saw-tooth' flights, data were averaged over the entire flight. Exponential curves were fitted to the collected data and extrapolated to determine the expected number of drops with radii between 400 μm and 1.7 mm, as these occur in small quantities and are poorly sampled by the optical array probe. In 80% of the cases, corrections produced a less than 2.5 dBZ enhancement of Z, though Z increased by 7.5 dBZ or more in 4% of the cases. O'Connor *et al.* (2004) also found that the exponential distribution reasonably described stratocumulus drizzle.

(*c*) *Data from C-band and millimetre cloud radars*

Radar data in this paper are from a 6-day observational period during EPIC Sc, 16–21 October 2001 inclusive, at 20°S, 85°W. This period was characterized by persistent Sc, sometimes continuous and other times broken, with intermittent drizzle throughout. One of the two meteorological radars aboard the RHB, the horizontally scanning C-band radar, has a 5 cm wavelength with 0.95° beam width (Ryan *et al.* 2002). It provided a reflectivity volume of 30 km radius every 5 minutes throughout EPIC Sc. The C-band lower reflectivity limit is about -12 dBZ at 30 km, sufficient to detect drizzle but not non-precipitating clouds. The upper limit is significantly higher than any reflectivity found in drizzle. Appendix A discusses the calibration, scan strategy, and the interpolation procedure applied to the C-band data. The calibration uncertainty is ± 2.5 dBZ. Quality-controlled C-band three-dimensional (3-D) reflectivity was averaged between 0.5 and 2 km and subsequently treated as a 2-D dataset. This vertical averaging was to circumvent uncertainties in radar pointing angles during volume scans, that produced uncertainties in the altitude corresponding to individual radar returns (see appendix A). Because the cloud thickness was typically less than the 500 m interpolated resolution, and data below 500 m were contaminated by sea clutter, vertical averaging did not significantly degrade reflectivity information.

The NOAA ETL 8.6 mm wavelength vertically pointing MMCR has a 0.5° beam width, and obtained a profile every 10 s during EPIC Sc. Its minimum detectable reflectivity is approximately -60 dBZ; the maximum depends on the distance from the radar, but it is about 20 dBZ near cloud top during EPIC (Moran *et al.* 1998). Uncertainties in MMCR data are outlined in appendix A. An example of C-band and MMCR data during EPIC Sc is shown in Bretherton *et al.* (2004, their Fig. 6).

(*d*) *Data from additional shipboard instrumentation*

A shipboard ceilometer provided cloud-base heights with 15 m vertical resolution at 15 s intervals. Hourly cloud-base heights were computed using the median value during each hour to eliminate the influence of spuriously low readings caused by drizzle.

Continuous observations were made of the vertically integrated cloud liquid-water content (i.e. the liquid-water path, *LWP*) using a microwave radiometer (Fairall *et al.* 1990; Bretherton *et al.* 2004). Data contaminated due to wetting of the radome

surface by drizzle were removed. There was also a broadband short-wave radiometer, or pyranometer, aboard the RHB (Bretherton *et al.* 2004).

3. Computation of Z–R relationships for drizzle at cloud base and the surface

Rain rates can be determined along aircraft flight paths using *in situ* DSD measurements, but current remote-sensing technology does not enable rain rate to be measured directly. Remote-sensing techniques can measure radar reflectivity, and radar reflectivities are converted into rain rates using a Z–R relationship traditionally of the form:

$$Z = aR^b, \tag{1}$$

where Z is the independent variable, and a and b are constants. Currently there are very few Z–R relationships published for drizzle. Reported slopes, b, in the literature vary widely from 1.0 (Vali *et al.* 1998) to 1.5 (Joss *et al.* 1970).

(*a*) *Z–R relationships for drizzle from DSDs*

The derivation of Z–R relationships from DSD data usually has fewer sources of uncertainty than other methods (e.g. radar–rain-gauge comparisons), because the data used to calculate both Z and R are obtained from the same volume of the atmosphere at the same time. However, short duration DSDs are typically not accurately sampled over the full range of relevant drop sizes (Joss and Gori 1978; Smith *et al.* 1993).

For the filter-paper DSDs, R and Z were estimated for each sample following Rinehart (1997). Aircraft Z and R were determined from the exponentially extrapolated DSDs as outlined in Rogers and Yau (1989). The relationship for terminal velocity used in these calculations is a function of drop radius, temperature, and pressure using the spherical best-number approach summarized in Pruppacher and Klett (1997).

Coefficients a and b can be obtained by least-squares regression of the logarithm of (1): $\log Z = \log a + b \log R$ (e.g. Doelling *et al.* 1998). If the correlation between Z and R is not close to unity, the values of a and b will vary depending on whether $\log Z$ or $\log R$ is treated as the independent variable (e.g. Campos and Zawadzki 2000). As we want to minimize errors in rain rate, we consider $\log Z$ to be the independent variable in all subsequent linear regressions, and rearrange the above terms to obtain

$$\log R = \frac{1}{b}(-\log a + \log Z). \tag{2}$$

Because values of $\log a$ are approximately normally distributed in our datasets, the one standard deviation (σ) values of $\log a$, corresponding to the 16th and 84th percentile values of a, can be used as error bounds on the Z–R relationship (Doelling *et al.* 1998).

Using this procedure, the surface Z–R relationship for the EPIC filter-paper data is $Z_{\mathrm{sfc}} = 57R_{\mathrm{sfc}}^{1.1}$, with the estimated error bounds $Z_{\mathrm{sfc}} = 38R_{\mathrm{sfc}}^{1.1}$ and $Z_{\mathrm{sfc}} = 86R_{\mathrm{sfc}}^{1.1}$. TEPPS filter-paper DSDs are also well described by this relationship. For the aircraft data, the resulting cloud-base relationship is $Z_{\mathrm{CB}} = 32R_{\mathrm{CB}}^{1.4}$, bounded by a values of 17 and 61*. A table of statistics for each dataset is presented in appendix B. Filter-paper and aircraft data are plotted in Fig. 1.

* If $\log R$ is considered the independent variable, the Z–R relationship is unchanged for the filter-paper, but the resulting aircraft relationship is $Z_{\mathrm{CB}} = 14R_{\mathrm{CB}}^{1.2}$.

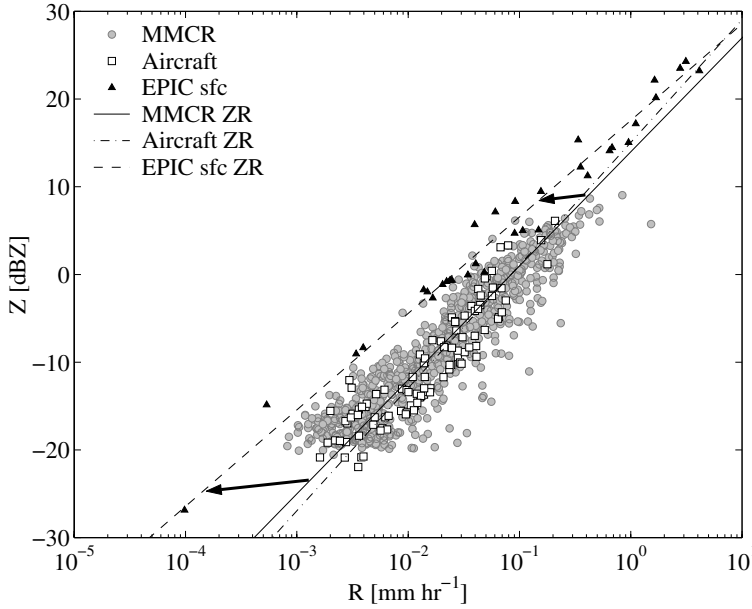

Figure 1. Reflectivity, Z, versus rain rate, R, for cloud-base millimetre-wavelength cloud radar (MMCR)-derived data (circles), cloud-base aircraft data (squares), and surface EPIC filter-paper data (triangles). Z–R relationship lines are shown for: MMCR $Z_{\mathrm{CB}} = 25R_{\mathrm{CB}}^{1.3}$ (solid); aircraft $Z_{\mathrm{CB}} = 32R_{\mathrm{CB}}^{1.4}$ (dashed); and filter-paper $Z_{\mathrm{sfc}} = 57R_{\mathrm{sfc}}^{1.1}$ (dash-dot). Arrows are sketched to represent evaporation between cloud base and the surface. See text for details.

We do not expect the Z–R relationships from the cloud (aircraft) and surface (filter-paper) data to be the same because the data sources differ significantly. Also, significant evaporation occurs below the cloud, affecting the DSD and therefore the Z–R relationship; this will be discussed in the following sections.

In this paper, we find $b = 1.1$–1.4. For deep convective rain, $b \cong 1.5$ (Smith and Joss 1997; Doelling *et al.* 1998; Steiner and Smith 2000). Other published Z–R relationships for drizzle include $Z = 150R^{1.5}$ (Joss *et al.* 1970) and $Z = 10R^{1.0}$ (Vali *et al.* 1998). Joss *et al.* acquired surface DSDs with a disdrometer but assumed the exponent in the Z–R relationship a priori to be 1.5, based on relationships available at that time for rain. Although we find a similar Z–R relationship for EPIC filter-paper DSDs when we assume $b = 1.5$, the Joss data may have been contaminated with ice within the cloud, which can alter the size distribution. Vali *et al.* used aircraft data from marine stratus off the Oregon coast. The small sample volume of the instrument (similar to the aircraft instrumentation described in subsection 2(b)) did not permit detection of any drops with radii larger than about 0.18 mm. Because larger drops have a disproportionate effect on reflectivity ($\sim D^6$, where D is drop diameter) compared to rain rate ($\sim D^4$), neglecting them introduces errors in the Z–R relationship. Appendix B shows the effect of extrapolation on the Z–R relationship.

(*b*) *Z–R relationships for drizzle from MMCR vertical profiles of reflectivity*

Because drizzle drops are small—rain rate and radar reflectivity in Sc are dominated by drops with radii in the range $20 < r < 400$ μm (Wood 2005)—their evaporation below cloud base will change the Z–R relationship. This has important implications for estimation of precipitation. To evaluate this effect, we use an evaporation–sedimentation

model that modifies the DSD (and thus Z and R) with distance beneath the cloud. We estimate the drizzle drop number concentrations N_D and the mean radii $\overline{r}$ of the DSDs by comparing MMCR reflectivity profiles with model results. This process yields another cloud-base Z–R relationship (from MMCR Z, and model-derived R) as well as relationships between cloud-base Z and below-cloud R.

(i) *Sedimentation–evaporation model: Evaporation of drizzle below cloud base.* The sedimentation–evaporation model simulates the evaporation of drizzle drops below cloud base. It does not include the effects of coalescence or break-up, but these effects are of little consequence below cloud for the sizes and concentrations of drizzle drops in Sc (Pruppacher and Klett 1997). The model provides steady-state solutions for a population of sedimenting drops evaporating into a sub-saturated environment below cloud base, with an imposed relative-humidity gradient of 0.36 km^{-1} based on EPIC observations. The DSD at cloud base is prescribed, and is represented by an exponential distribution truncated at a lower size limit, r_0, shown to be a good fit by Wood (2005):

$$N_{CB}(r) = \frac{N_D}{\overline{r} - r_0} \exp\{-(r - r_0)/(\overline{r} - r_0)\} \quad (r > 20\ \mu\mathrm{m}), \tag{3}$$

where $\overline{r}$ is the mean radius of the truncated exponential distribution *at cloud base**, and $r_0 = 20\ \mu$m is the smallest drizzle drop size. Drops smaller than r_0 are cloud drops with insignificant terminal velocities and negligible contributions to radar reflectivity. Including the small drops can result in instabilities in the model because their evaporation rates are large. Model details and a discussion of the limitations of the technique are presented in appendix C.

The following function provides a reasonable parametrization of the model-predicted rainfall rate as a function of height above the surface, z, for a truncated-exponential DSD†:

$$\frac{R(z)}{R_{CB}} = c(\chi) = \exp(-k\chi(\overline{r}, z)), \tag{4}$$

where $\chi = \{(z_{CB} - z)/(\overline{r})^{2.5}\}^{1.5}$ is a normalized height coordinate. R_{CB} is rain rate at cloud base, i.e. where $z = z_{CB}$. A single value of constant $k = 320\ \mu\mathrm{m}^{3.75}\mathrm{m}^{-1.5}$ was found to be appropriate for the temperatures, pressures and vertical relative-humidity gradients observed during EPIC Sc (see appendix C).

The model can be used to estimate changes to the Z–R relationship as the drizzle evaporates. For the range of cloud-base mean radii observed in drizzling Sc, the model-predicted reflectivity can be further parametrized:

$$\frac{Z(z)}{Z_{CB}} \approx \left(\frac{R(z)}{R_{CB}}\right)^q, \tag{5}$$

where $q \approx 0.75$ for our simulations of drizzle evaporation. Reflectivity decreases more slowly with distance below cloud base than does the precipitation rate, because the dominant contributions to the reflectivity are from larger, more slowly evaporating droplets than those that dominate the rain rate.

* For a non-truncated exponential the ratio of mean volume radius, r_{vol}, to $\overline{r}$ is $6^{(1/3)} = 1.8$. For an exponential truncated at radius r_0, the ratio $r_{vol}/\overline{r}$ is lower than this and increases with the ratio $\overline{r}/r_0$. For $r_0 = 20\ \mu$m, $\overline{r} = 30\ \mu$m corresponds to $r_{vol} = 34\ \mu$m, and $\overline{r} = 50\ \mu$m corresponds to $r_{vol} = 67\ \mu$m. Aircraft measurements (Wood 2005) find r_{vol} at the cloud base between 31 and 53 μm consistent with this range.

† The authors note that our evaporation–sedimentation model can be solved analytically by separation of variables to yield solutions having a Weibull-type distribution, from which a linear combination of solutions could be used, in theory, to match the prescribed boundary conditions at the cloud base. However, the incorporation of the exponential distribution boundary condition at $z = z_{CB}$ would lead to unwieldy mathematical solutions.

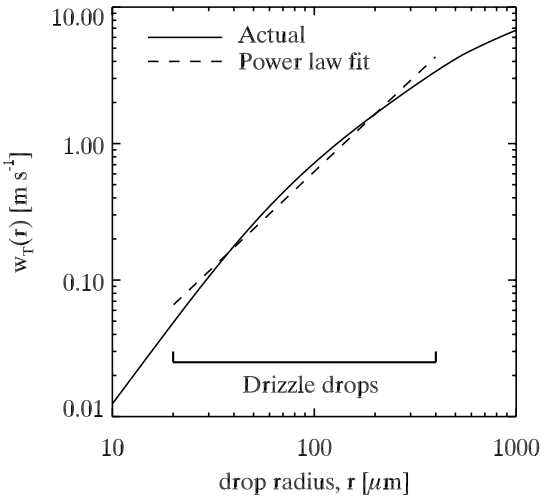

Figure 2. Terminal-velocity relationship with drizzle drop radius from Pruppacher and Klett (1997) (actual, solid line), and single power law used to fit the velocity relationship (dashed line) for simplifying calculations.

The value of q is primarily a function of the relationship between terminal velocity and drop size, but it also depends on the form of the assumed DSD and on the relationship between evaporation rate and drop size. The exponent may be somewhat different in other types of rain-producing systems, such as deep-convective or midlatitude rain. Approximately, $q = (3 + d)/6$, where d is the exponent in the relationship between terminal velocity, ω_T, and drop size:

$$\omega_T(r) = A_T r^d, \tag{6}$$

with $A_T = 2.2 \times 10^5$ m$^{-0.4}$s^{-1} and $d = 1.4$ (for r in m and ω_T in m s^{-1}). This relationship, shown in Fig. 2, provides a reasonable fit to the terminal-velocity relations given in Pruppacher and Klett (1997) for the size range $20 < r < 400$ μm. This single power law in (6) simplifies the solution of the sedimentation–evaporation equations, and tests indicate that results do not appreciably differ from those obtained using a more complex form. The exponent d here is different from that for rain (e.g. Rogers and Yau 1989) because it is optimized to drops of smaller size.

Combining (4) and (5) gives:

$$\frac{Z(z)}{Z_{CB}} = \exp(-qk\chi(\overline{r}, z)). \tag{7}$$

To show that the parametrization (7) is consistent with independent *in situ* data, we plot aircraft estimated reflectivity data against χ in Fig. 3. No *in situ* cloud microphysical measurements were made during EPIC Sc, but we consider Sc clouds sufficiently universal in nature for the UK results to serve as a test of the numerical model. Relative-humidity gradients are similar to those in EPIC Sc (within $\pm 10\%$). Although the observed values are somewhat scattered due to sampling uncertainties and variable cloud-base heights, the model parametrization (7) does not seem unduly biased, and represents the observations well.

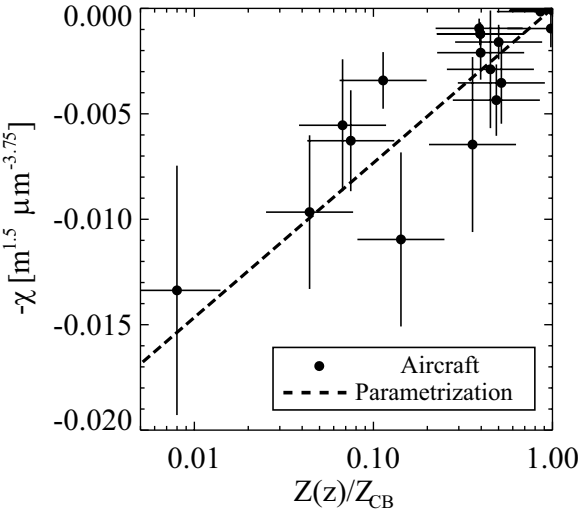

Figure 3. Profiles of radar reflectivity, Z, below cloud normalized with the maximum value, Z_{CB}, versus the normalized height variable $\chi = \{(z_{\mathrm{CB}} - z)/(\overline{r})^{2.5}\}^{1.5}$. Circles represent aircraft data from the UK Met Office flights in North Atlantic Sc with estimated error bars. The dashed line shows the evaporation–sedimentation model parametrization using (7). See text for details.

(ii) *MMCR-based estimation of cloud-base drizzle parameters and a Z–R relationship.* The MMCR cloud-base reflectivity and profiles below cloud base are combined with the parametrization from the sedimentation–evaporation model to estimate the parameters of the drizzle DSD at cloud base. The latter is assumed to be a truncated exponential function. To avoid contributions from cloud liquid water, no profile with a maximum reflectivity less than −20 dBZ was used. We averaged the acceptable profiles over 10 minutes, because this is short enough to capture the spatial variability of drizzle observed during EPIC and long enough to ensure that the profile would be vertically coherent with respect to the falling of drizzle drops. We approximate cloud base as the height with maximum reflectivity in the MMCR profile in order to simplify the exponential fit (7). The mean height of the maximum reflectivity is consistent with the cloud base derived from the ceilometer. Figure 4 shows three example MMCR profiles compared with parametrization (4) and the cloud bases for cases of light and heavy drizzle.

For each 10-minute mean MMCR reflectivity profile, we solve for $\overline{r}$ in (7) using the $Z(z)/Z_{\mathrm{CB}}$ profile between cloud base and 400 m. Only data in this height range are used, to ensure that (7) is a good approximation and to avoid problems associated with the saturation of the MMCR at low levels.

Once $\overline{r}$ is known, N_{D} is derived using the observed cloud-base radar reflectivity $Z_{\mathrm{CB}} = 2^6 M_6$, where M_6 is the 6th moment of a truncated exponential distribution. The moments M_n of order n of this distribution can be expressed, using an integral recurrence relation, as

$$M_n(r_0, \overline{r}, N_{\mathrm{D}}) = N_{\mathrm{D}} n!(\overline{r} - r_0)^n \sum_{i=0}^{n} \left(\frac{r_0}{\overline{r} - r_0}\right)^i \frac{1}{i!}. \tag{8}$$

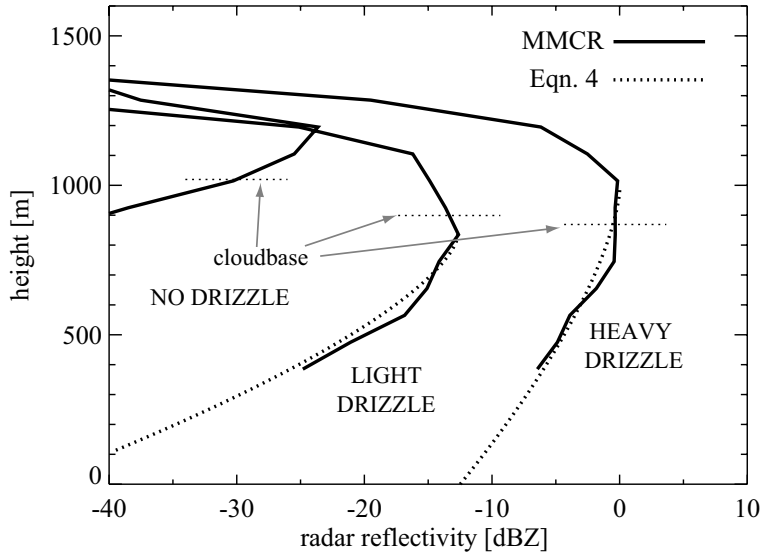

Figure 4. Ten-minute mean profiles of millimetre-wavelength cloud radar (MMCR) reflectivity with the model parametrization (4), and ceilometer cloud-base heights. Profiles are representative of typical conditions with no drizzle, light drizzle, and heavy drizzle during EPIC. Peak reflectivity occurs at cloud base during drizzling periods but somewhat higher in non-drizzling periods.

Once $\overline{r}$ and N_{D} are found, any of the moments of the truncated exponential distribution can be obtained through (8). For example, the rain rate at cloud base is

$$R_{\mathrm{CB}} = \frac{4\pi\rho_{\mathrm{w}}}{3} A_{\mathrm{T}} M_{d+3}(r_0, \overline{r}, N_{\mathrm{D}}), \tag{9}$$

where A_{T} and d are from (6) (the approximation for the terminal velocity of drizzle drops) and ρ_{w} is the density of water. For non-integer values of d we interpolate (8) to find M_{d+3}. Figure 5 shows time series of N_{D} and $\overline{r}$ and their median fitting uncertainties from the model based on MMCR data during EPIC Sc. The range of variations in $\overline{r}$ is small (40 ± 20 μm) compared to N_{D}, which fluctuates over four orders of magnitude.

A Z–R relationship is computed as described in subsection 3(a) from cloud-base R_{CB} estimated using (9) and MMCR Z_{CB}:

$$Z_{\mathrm{CB}} = 25 R_{\mathrm{CB}}^{1.3}, \tag{10}$$

with uncertainty bounds in a of 11 and 54*. Figure 1 shows MMCR Z_{CB} and R_{CB} values together with (10).

(iii) *Effect of evaporation below cloud: bi-level Z–R relationships.* Cloud-base Z–R relationships can be applied to the cloud-base radar data to determine the amount of drizzle falling out of the clouds, but how much drizzle reaches the surface? The evaporation–sedimentation model predicts drizzle rates at any level below the cloud by modifying the inferred cloud-base DSDs from the MMCR data. From the model-derived rain-rate profiles we can estimate 'bi-level' Z–R relationships that relate cloud-base reflectivity to below-cloud rain rates.

To explore what we expect a bi-level Z–R relationship to look like, we use (4) and assume the Z–R relation obeys a power law, i.e. $Z_{\mathrm{CB}} = aR_{\mathrm{CB}}^{b}$ at cloud base, which leads

* Using $\log(R)$ as the independent variable would yield an alternative relationship: $Z_{\mathrm{CB}} = 11 R_{\mathrm{CB}}^{1.1}$.

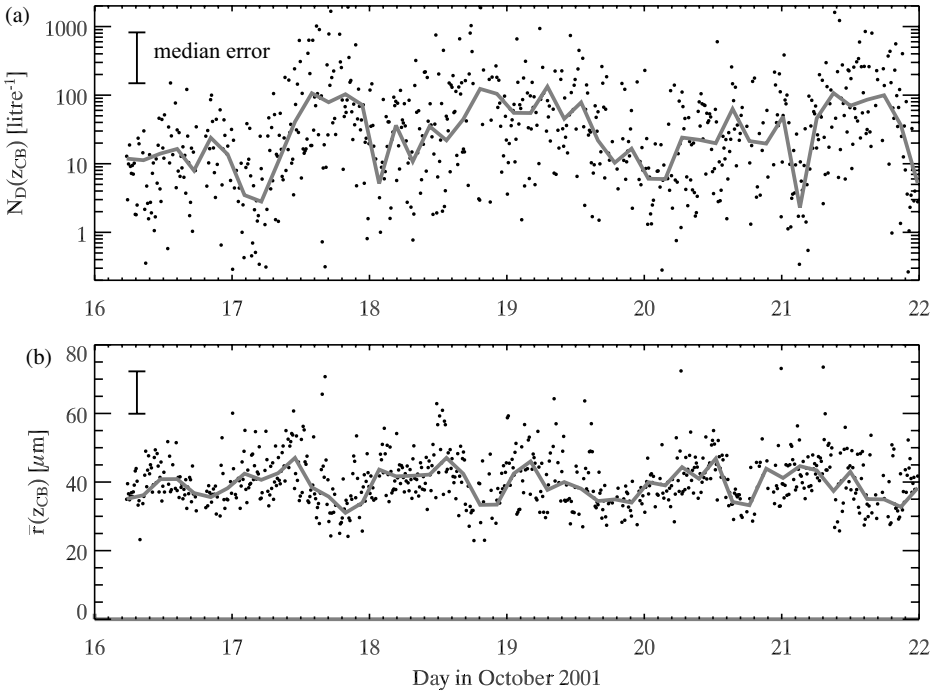

Figure 5. Time series of: (a) 10-minute cloud-base drizzle drop concentration $N_D(z_{CB})$, and (b) mean cloud-base drizzle drop radius $\overline{r}(z_{CB})$, derived using millimetre-wavelength cloud radar reflectivity profiles (dots). Lines show 3-hourly mean values. Median error bars in each plot represent uncertainties in N_D and $\overline{r}$. Time is UTC.

to

$$Z_{CB} = a\left(\frac{R(z)}{c(\chi)}\right)^b. \tag{11}$$

Taking the logarithm of (11) and using the definition of $c(\chi)$ gives

$$\log Z_{CB} = \log a + b\{\log R(z) + k\chi(\overline{r}, z)\}. \tag{12}$$

It is apparent from (12) that there is not necessarily a simple power-law relationship between Z at cloud base and R below cloud. This is not surprising, because evaporation changes the size distribution and affects reflectivity and rain rate nonlinearly (see section 4(a)). From our data, it is reasonable to expect that the departure from linearity increases with increasing distance from the cloud base, or increasing evaporation.

The range of rain rates is limited in the MMCR 10-minute average dataset, and is insufficient to fully define a non-power-law Z–R relationship for all rain rates of interest; hence, instead we define a piecewise linear function. Only profiles with below-cloud rain rates greater than 1×10^{-4} mm hr^{-1} are used because of the large scatter and insignificant accumulation associated with lower rain rates (see subsection 5(b)). The relation is estimated by assuming a linear relationship between $\log Z_{CB}$ and $\log R(z)$ below cloud, as in (2). Where this Z–R line intersects the cloud-base Z–R line it must follow the latter for higher reflectivity values, because in an evaporative environment there cannot be more precipitation below cloud than at cloud base. The $\log R(z)$ data are obtained by using the model to sediment/evaporate the MMCR estimated cloud-base DSD. Model-derived surface rain rates and several bi-level Z–R relationships are shown in Fig. 6.

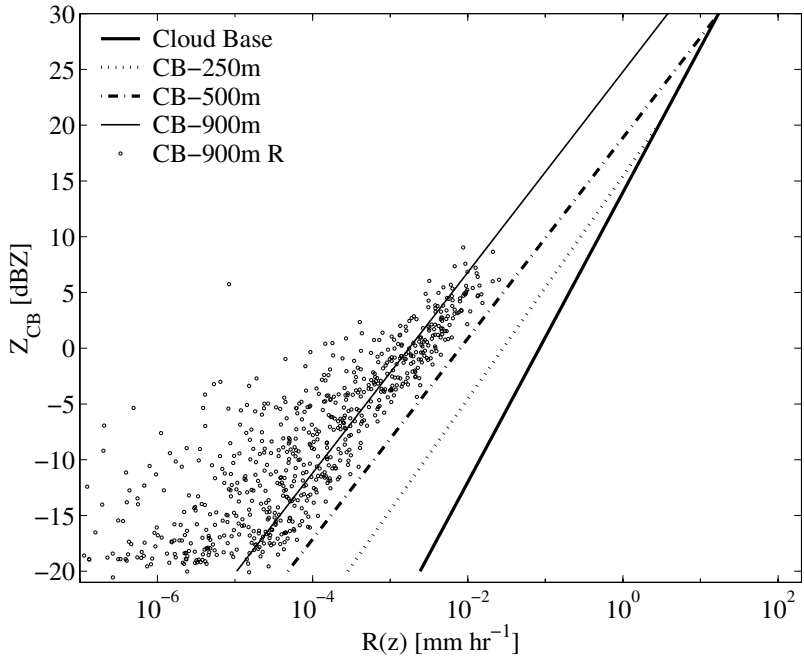

Figure 6. Bi-level relationships of radar reflectivity, Z, and rainfall rate, R, from the evaporation–sedimentation model at various levels: at the cloud base ($Z_{CB} = 25R_{CB}^{1.3}$); 250 m below cloud base ($Z_{CB} = 35R(z_{CB\text{-}250})^{1}$); 500 m below cloud base ($Z_{CB} = 75R(z_{CB\text{-}500})^{0.9}$); and 900 m below cloud base, which is the average distance to the surface, ($Z_{CB} = 302R_{sfc}^{0.9}$). Circles represent model-derived rain rates at 900 m below cloud base. Relationships were calculated using $R(z) \geqslant 10^{-4}$ mm hr^{-1}, although they are plotted for lower rain rates here. See text for details.

Increasing the distance below cloud increases the rain rate at which the bi-level and cloud-base Z–R relations intersect, i.e. the maximum rain rate at which measurable evaporation occurs between cloud base and the specified level. The average cloud base during EPIC was around 900 m (Bretherton *et al.* 2004), so the 'surface' (CB–900 m) bi-level Z–R relation, is:

$$Z_{CB} = 302R_{sfc}^{0.9}, \tag{13}$$

with uncertainty bounds in a of 159 and 571.

Although the derived bi-level Z–R relationships may not be precise descriptions of the sub-cloud rain-rate behaviour, our results show an important trend in the relationship between cloud-base reflectivity and below-cloud rain rates. For low rain rates at cloud-base, it is essential to consider the evaporation below cloud base when relating rain rate and reflectivity at different levels (Li and Srivastava 2001).

(iv) *Potential sources of error in the derived drizzle parameters.* Two categories of uncertainty lead to errors in the derived drizzle parameters. The first category, discussed in appendix A, is related to possible saturation of the MMCR. Periodic MMCR saturation means that there are no high values of reflectivity to constrain the MMCR-derived Z–R relation. This may lead to poor estimates of rain rate for the highest reflectivity values that are measured by the C-band radar. The second source of error, discussed in appendix C, arises from simplifying assumptions made in the method of estimation of drizzle parameters from the MMCR reflectivity profiles.

An important assumption made in the model is that vertical air motions have negligible effect on the profiles of rain rate and reflectivity, and on their dependence upon the mean radius of the drizzle drops at cloud base. It is well understood (e.g. Nicholls 1987) that the terminal velocity of drizzle drops is comparable to the vertical ascent/descent rates for turbulent eddies, and that this motion has an important effect on the production of drizzle by recirculating small drizzle drops within the cloud. It is less certain how this may impact the rain-rate profiles below cloud where many of the smaller drops have evaporated. Because our method uses 10-minute mean profiles, the mean vertical motion over this period will be negligible because the typical duration of a eddy of scale 1000 m as it passes over the ship is about 2 minutes. However, a non-zero correlation between $\overline{r}$ and vertical wind at smaller scales would alter the profile (4), leading to overestimates in rain rate. These errors are estimated to be smaller than those associated with the uncertainty in C-band radar calibration (see appendices A and C).

4. Understanding the parameters in the Z–R relationship

(*a*) *Expected changes in Z–R relationships due to evaporation*

The Z–R relationships for the surface and cloud base differ in part because of the nature of the DSD collection, but the main source of difference is due to evaporation below cloud base. From the cloud-base and surface Z–R lines shown in Fig. 1, we see that a increases significantly from cloud base to the surface, while the exponent decreases slightly. Parcels with higher rain rates tend to be less affected by evaporation than parcels with lower rain rates, as represented by arrows in Fig. 1. Some surface Z values in Fig. 1 are greater than the cloud-base values, primarily because filter-paper samples are nearly instantaneous while cloud-base samples are horizontally averaged (see also MMCR uncertainties in appendix A).

(*b*) *Mathematical derivation of b*

We can understand the cloud-base Z–R relationship in terms of the joint probability density function (pdf) of drizzle drop concentration, N_{D}, and mean drizzle drop radius, $\overline{r}$. Figure 7 shows scatter plots of pair-wise correlations among MMCR-derived 10-minute averaged N_{D}, $\overline{r}$, and cloud-base rain rate, R_{CB}, obtained as in subsection 3(b)(ii). The correlation coefficients between the logarithms of these variables are 0.72 (N_{D}, R), −0.58 (N_{D}, $\overline{r}$) and 0.14 ($\overline{r}$, R), the latter of which is not significant. We can now use this information to derive an expression for the value of the exponent b in the Z–R relationship at cloud base, $Z_{\mathrm{CB}} = aR_{\mathrm{CB}}^{b}$. Relating Z and R to the moments of a truncated exponential DSD:

$$\begin{aligned} Z_{\mathrm{CB}} &= \alpha_1 M_6 \\ R_{\mathrm{CB}} &= \alpha_2 M_{d+3}, \end{aligned} \tag{14}$$

where α_1 and α_2 are constants with values of 2^6 and $\frac{4}{3}\pi\rho_{\mathrm{w}}A_{\mathrm{T}}$ from (9), respectively, and M is from (8). Using a power-law fit to (8) over the estimated range $25 < \overline{r} < 60$ μm, we obtain:

$$\begin{aligned} M_6 &\approx N_{\mathrm{D}}(\overline{r})^{\beta_1} \\ M_{d+3} &\approx N_{\mathrm{D}}(\overline{r})^{\beta_2}, \end{aligned} \tag{15}$$

where $\beta_1 \approx 9.8$ and $\beta_2 \approx 6.5$ if $r_0 = 20$ μm. Without truncation of the exponential size distribution, i.e. $r_0 = 0$, we would obtain $\beta_1 = 6$ and $\beta_2 = 3 + d$ (and (15) would be exact).

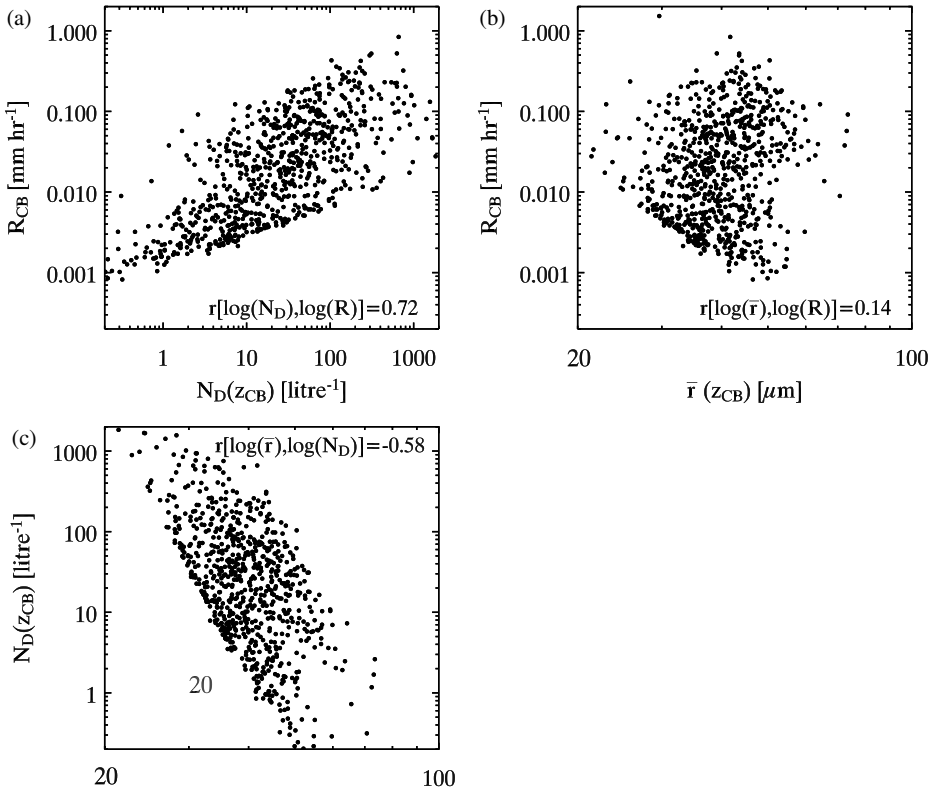

Figure 7. Correlations between: (a) drizzle drop concentration, N_D, and rain rate, R; (b) drizzle drop mean radius, $\overline{r}$, and R; and (c) $\overline{r}$ and N_D, for parameters at cloud base derived by millimetre-wavelength cloud radar. Correlations greater than 0.35 are significant at the 95% confidence level.

The parameters $\log a$ and b in the Z_{CB}–R_{CB} power law (2) can be considered optimal least-squares values obtained from the regression of $\log R_{CB}$ on $\log Z_{CB}$. Together, (14) and (15) express Z_{CB} and R_{CB} in terms of N_D and $\overline{r}$. We can deduce expressions for $\log a$ and b in terms of the fluctuations in these two DSD parameters if they have a bivariate log-normal joint pdf, with a correlation coefficient $r_{\log N_D \log \overline{r}}$. The solution for the least-squares value of b at cloud base is:

$$b = \frac{1}{r_{\log R \log Z}} \left\{ \frac{1 + \beta_1^2 \sigma^2_{\log \overline{r}} / \sigma^2_{\log N_D} + 2\beta_1 r_{\log \overline{r} \log N_D} \sigma_{\log \overline{r}} / \sigma_{\log N_D}}{1 + \beta_2^2 \sigma^2_{\log \overline{r}} / \sigma^2_{\log N_D} + 2\beta_2 r_{\log \overline{r} \log N_D} \sigma_{\log \overline{r}} / \sigma_{\log N_D}} \right\}^{\frac{1}{2}}, \qquad (16)$$

where $\sigma^2_{\log N_D}$ and $\sigma^2_{\log \overline{r}}$ are the variances of the logarithms of N_D and $\overline{r}$, which indicate the respective degrees of variability of the size distribution parameters (see appendix D for derivation). Thus, the exponent is determined by the relative amount of variance in N_D and $\overline{r}$ (see also Doelling *et al.* 1998). Note that the degree of correlation between $\log \overline{r}$ and $\log N_D$, $r_{\log \overline{r} \log N_D}$, does not greatly affect b, and the correlation between $\log R$ and $\log Z$, $r_{\log R \log Z}$, is typically close to one. The two limiting cases (assuming for the moment that $\log Z$ and $\log R$ are perfectly correlated and there is no correlation between $\log \overline{r}$ and $\log N_D$) are: $b = 1$ (precipitation rate variations are dominated by variations in N_D, $\sigma^2_{\log N_D} \gg \sigma^2_{\log \overline{r}}$), and $b = (\beta_1/\beta_2) = 1.51$ (precipitation rate variations

TABLE 1. VALUES OF DROP SIZE DISTRIBUTION PARAMETERS AND THEIR VARIABILITY

Parameter	Value (EPIC MMCR)	Value (Aircraft)	Units
$\sigma_{\log N_D}$	0.787	0.628	None
$\sigma_{\log \overline{r}}$	0.082	0.161	None
Median N_D	2.35×10^4	2.54×10^4	m^{-3}
Median $\overline{r}$	39.3	34.5	μm
$r_{\log R \log Z}$	0.92	0.91	None
$r_{\log \overline{r} \log N_D}$	−0.58	−0.44	None

See text for details.

TABLE 2. RELATIVE CONTRIBUTIONS TO VARIANCE IN RAINFALL RATE, R, AND RADAR REFLECTIVITY, Z

Contribution	to variance of R	to variance of Z
from N_D	0.62	0.62
from $\overline{r}$	0.29	0.66
from $r_{\log N_D \log \overline{r}}$	−0.49	−0.74
Sum	0.42	0.54
Observed	0.42	0.56

See text for details.

are entirely modulated by variations in $\overline{r}$, $\sigma^2_{\log \overline{r}} \gg \sigma^2_{\log N_D}$)*. Equation (16) couches the Z–R exponent b as a physically significant parameter related to whether variability (in time or space) in drizzle droplet number concentration or in the size of the drops has most influence over variability in the precipitation rate. A similar relationship is shown graphically in Steiner *et al.* (2004) based on modelled DSD data. Relevant quantities for the estimation of b for both MMCR-derived and aircraft data are given in Table 1.

Distributions of N_D and $\overline{r}$, calculated from the MMCR data, are approximately log-normal. Log-variances for the MMCR-derived size-distribution parameters (Table 1), lead to a theoretical value (16) of $b = 1.24$. This is intermediate between the limiting values, indicating that precipitation rate variability is controlled by variability in both N_D and $\overline{r}$. There is much greater variability in N_D but, because of the stronger dependence of Z on r (compared to R), $\overline{r}$ also impacts the fluctuations in radar reflectivity and, to a lesser degree, in rain rate. The aircraft data were characterized by higher variation in $\overline{r}$, which led to a larger theoretical b of 1.41.

To better understand the relative contributions of N_D and $\overline{r}$ to variances in R and Z, the variance equation for log Z or log R can be written $\sigma^2_{\log(Z \text{ or } R)} = \sigma^2_{\log N_D} + \beta^2 \sigma^2_{\log \overline{r}} + 2\beta r_{\log N_D \log \overline{r}} \sigma_{\log N_D} \sigma_{\log \overline{r}}$ where $r_{\log N_D \log \overline{r}}$ is a correlation coefficient, and β is either β_1 (for Z) or β_2 (for R). Results given in Table 2 indicate that the values of β_1 and β_2 are appropriate, because the sum of the terms is very close to the observed variance in the MMCR-derived time series. These are not always equal because (15) is not exact. Variability in N_D contributes more than $\overline{r}$ for R, but for Z both contribute more equally. The negative correlation between N_D and $\overline{r}$ reduces the variance in R and Z.

* In the classic Marshall–Palmer formulation (Marshall and Palmer 1948), their N_0 (our $N_D/\overline{r}$) is taken to be a constant. This implies that $\sigma_{\log \overline{r}} = \sigma_{\log N_D}$ and $r_{\log \overline{r} \log N_D} = 1$. The value of $r_{\log R \log Z}$ also equals one for a Marshall–Palmer distribution. Inserting those values into (16) with the definitions for β_1 and β_2 for untruncated distributions, $b = (1 + \beta_1)/(1 + \beta_2) = (1 + 6)/(1 + 3 + d)$. For rain $d = 0.67$ (Gunn and Kinzer 1949), so the theoretical exponent b equals the expected value of 1.5.

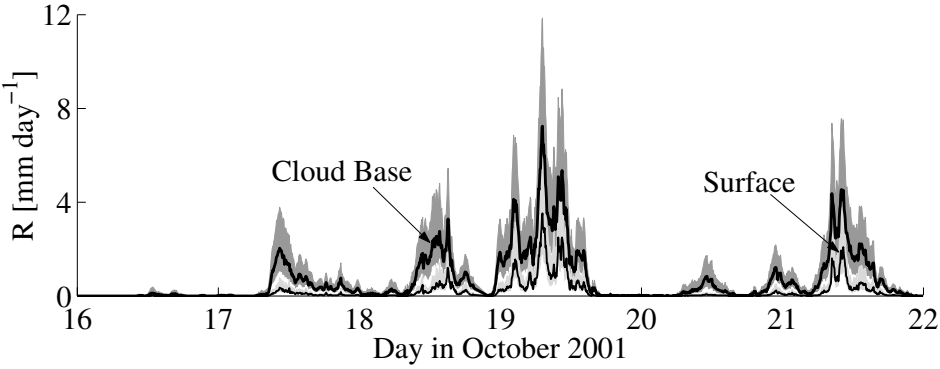

Figure 8. Estimated areal average rain rate from C-band radar data for the cloud base and surface from millimetre-wavelength cloud radar-derived cloud-base and bi-level relationships of radar reflectivity and rain rate (Z–R) for 6 days during EPIC Sc. Shading represents C-band calibration uncertainties of ±2.5 dBZ. Time is UTC.

5. IMPLICATIONS

(*a*) *Estimation of drizzle amount from radar data*

Previous sections have described methods to obtain relationships between observed radar reflectivity and precipitation at cloud base and below. These relationships can now be applied to determine the amount of rainfall during the EPIC Sc and TEPPS Sc cruises. To obtain area-averaged cloud-base rain rate, we apply the MMCR-derived Z–R relationship (10) to the C-band data, in order to take advantage of the C-band radar's superior areal coverage. The resulting area-averaged rain-rate time series during EPIC Sc is shown in Fig. 8. The surface drizzle rate, derived from the bi-level Z–R relationship (13), is also shown. The effect of the ±2.5 dBZ calibration uncertainty on the estimated rain rates is illustrated. This is the largest source of error in the rainfall estimation. The Z–R relationship uncertainties are not shown; they are of the same magnitude as the calibration uncertainties. Average reflectivity is determined using C-band data interpolated to 500 m by 500 m pixels. Because precipitation rates are scale-dependent, a different spatial resolution may yield somewhat different results.

For each Z–R relationship derived in this study, the average rainfall rate is computed for the days on which it drizzled during EPIC and TEPPS Sc in order to make a fair comparison between rain rates in the north-east and south-east Pacific Sc regions. 'Drizzle days' are defined as having a daily areal average rain rate (AARR) of >0.1 mm day^{-1} *or* a daily average conditional rain rate (ACRR) > 5 mm day^{-1}. The conditional rain rate describes the pixel rain rate if and only if it is raining. AARRs and ACRRs and uncertainties are presented in Table 3.

Our best estimate of the mean AARR during the 5 drizzle days in EPIC Sc is about 0.7 mm day^{-1} at cloud base, with a total uncertainty envelope of 0.2–2.3 mm day^{-1}. About 0.2 mm day^{-1} reached the surface (uncertainty range 0.1–0.6 mm day^{-1}). On the two TEPPS drizzle days there was much less precipitation, about 0.2 mm day^{-1} at cloud base (within the range 0.1–0.5 mm day^{-1}), and 0.1 mm day^{-1} (0.04–0.2 mm day^{-1}) at the surface.

During TEPPS, we expect the C-band calibration uncertainty to be in the same range as for EPIC. The TEPPS region was synoptically different from the EPIC Sc region, with a more decoupled MBL and higher cloud bases at times (as much as 200 m), so the surface rain rates may be slightly overestimated. Drizzle occurred less frequently during TEPPS, but when it was drizzling the cloud-base rain rates are comparable to

TABLE 3. AVERAGE AREA AND AVERAGE CONDITIONAL RAINFALL RATES FOR EPIC AND TEPPS

Daily areal average rain rate (AARR)	Z–R	EPIC			TEPPS		
		−2.5 dBZ	0 dBZ	2.5 dBZ	−2.5 dBZ	0 dBZ	2.5 dBZ
MMCR-derived − (CB)	$Z = 11R^{1.3}$	0.7	1.3	2.3	0.2	0.3	0.5
MMCR-derived (CB)	$\mathbf{Z = 25R^{1.3}}$	**0.4**	**0.7**	**1.3**	**0.1**	**0.2**	**0.3**
MMCR-derived + (CB)	$Z = 54R^{1.3}$	0.2	0.4	0.7	0.1	0.1	0.2
bi-level − ($R_{\rm sfc}$, $Z_{\rm CB}$)	$Z = 159R^{0.9}$	0.1	0.3	0.6	0.1	0.1	0.2
bi-level ($R_{\rm sfc}$, $Z_{\rm CB}$)	$\mathbf{Z = 302R^{0.9}}$	**0.1**	**0.2**	**0.4**	**0.0**	**0.1**	**0.1**
bi-level + ($R_{\rm sfc}$, $Z_{\rm CB}$)	$Z = 571R^{0.9}$	0.0	0.1	0.2	0.0	0.1	0.1
Daily average conditional rain rate (ACRR)							
MMCR-derived − (CB)	$Z = 11R^{1.3}$	10.4	12.0	13.7	13.8	16.3	18.8
MMCR-derived (CB)	$\mathbf{Z = 25R^{1.3}}$	**5.8**	**6.7**	**7.7**	**7.7**	**9.2**	**10.6**
MMCR-derived + (CB)	$Z = 54R^{1.3}$	3.3	3.8	4.3	4.3	5.1	5.9
bi-level − ($R_{\rm sfc}$, $Z_{\rm CB}$)	$Z = 159R^{0.9}$	0.4	0.7	1.4	1.0	1.7	2.9
bi-level ($R_{\rm sfc}$, $Z_{\rm CB}$)	$\mathbf{Z = 302R^{0.9}}$	**0.2**	**0.4**	**0.9**	**0.8**	**1.4**	**2.4**
bi-level + ($R_{\rm sfc}$, $Z_{\rm CB}$)	$Z = 571R^{0.9}$	0.1	0.3	0.5	0.7	1.1	2.0

MMCR is millimetre-wavelength cloud radar, CB is cloud base, sfc is surface, R is rain rate and Z radar reflectivity. Average rain rates in mm day^{-1} are given for: mean Z–R relationships, Z–R uncertainties and C-band calibration uncertainties (−2.5, 0, +2.5 dBZ) on EPIC Sc drizzle days (17–21 Oct. 2001) and TEPPS Sc drizzle days (2–3 September 1997). Best estimates from (10) and (13) are in bold. Only values of $R \geqslant 1 \times 10^{-4}$ mm hr^{-1} are used to compute daily rain rates. See text for further details.

those from EPIC (see ACRRs in Table 3). Even with the uncertainties, it is clear that a substantial amount of evaporation of sub-cloud drizzle is occurring in both the north-east and south-east Pacific Sc MBLs.

(*b*) *The spatial pdf of cloud-base drizzle rate*

As in deep convective rainfall (e.g. Doelling *et al.* 1998), the spatial pdf of drizzle rate is strongly skewed, such that a large percentage of the rain rate in drizzling Sc falls from only a small fraction of the area. This may lead to considerably different dynamical feedbacks than if the drizzle fell evenly throughout (through spatially patchy evaporative cooling in the sub-cloud layer and latent warming in the cloud layer). We examine spatial cloud-base rain-rate pdfs using the C-band radar data from EPIC Sc. The C-band radar has far better sampling statistics than the MMCR and gives true spatial variability information. For each C-band horizontal scan, the MMCR-derived Z–R relationship (10) is used to estimate rainfall at each pixel, and a pdf of rain rate is obtained. All of the pdfs are then composited. As illustrated in Fig. 9(a), the pdf of the drizzling area has a significant tail, which indicates that a considerable amount of rain is associated with only a small fraction of the area. For example, as shown in Fig. 9(b), 50% of the drizzle accumulation is contributed by rain rates greater than 0.37 mm hr^{-1}, but it originates from only 5% of the drizzling area. Drizzle was detected by the C-band in only 41% of the total area, so that 90% of the accumulation, which comes from 68% of this drizzling area, corresponds to only 28% of the total area. The intermittency is considerable. Because most of the drizzle during EPIC evaporated, and rates of 0.04 mm hr^{-1} can lead to local sub-cloud cooling rates of several K day^{-1}, it is possible that evaporating drizzle could result in downdraughts with subsequent dynamical response that may locally enhance cloud thickness and drizzle production (Jensen *et al.* 2000).

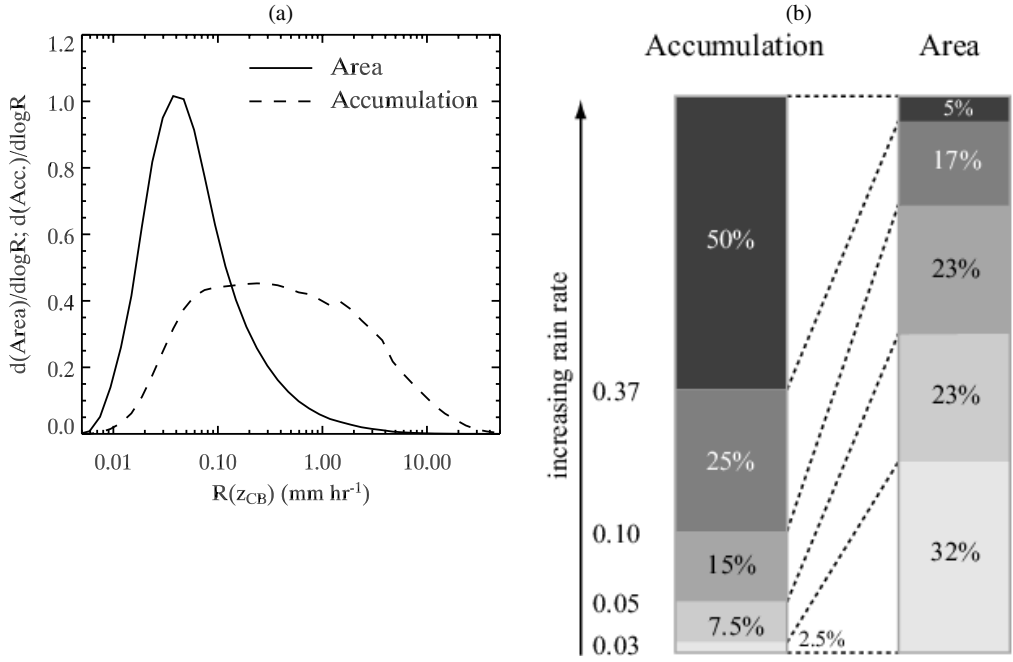

Figure 9. (a) Composite probability density functions of drizzling area (solid line) and total accumulation (dashed line) for each rain rate at cloud base, $R(z_{CB})$. Data are taken from the C-band radar using the relation (10) derived from millimetre-wavelength cloud radar. (b) The total rainfall accumulation and the corresponding drizzling area for the given rain rates (e.g. 25% of the rain comes from $0.10 < R(z_{CB}) < 0.37$ mm hr^{-1}, and this corresponds to 17 % of the drizzling area).

(*c*) *Estimation of rain rate from cloud-drop concentration and liquid-water path*

Model simulations (e.g. Nicholls 1987; Baker 1993; Austin *et al.* 1995; Khairoutdinov and Kogan 2000), observations (e.g. Bower *et al.* 1992) and simple physical arguments (Tripoli and Cotton 1980), show that the production of drizzle depends strongly upon both the cloud liquid-water content and the cloud droplet concentration, with high liquid-water content and low droplet concentration leading to stronger drizzle production. During EPIC Sc, the cloud droplet concentration, N_d (note that this is different from drizzle drop concentration, N_D, used previously), was estimated during the daytime using the observed *LWP* and cloud transmission measurements from the pyranometer (Dong and Mace 2003; Bretherton *et al.* 2004). Linear interpolation of the daytime N_d was used to estimate values during the night. Because of the coarseness in N_d estimations, and to reduce the sampling uncertainties, all the values (R_{CB}, *LWP*, and N_d) are aggregated into 3 h means. Air advects about 75 km in a 3 h period; during this time, patches of thicker and thinner cloud may advect overhead, resulting in considerable *LWP* variability. Thus, these estimates should be regarded as appropriate for mean quantities averaged over (75 km)^2 regions. Tests show that R_{CB} is reasonably well parametrized as a function of LWP/N_d (Fig. 10):

$$R_{CB} = 0.0156(LWP/N_d)^{1.75}, \tag{17}$$

with *LWP* in g m^{-2}, N_d in cm^{-3}, and R_{CB} in mm hr^{-1}. The correlation between rain rates derived in subsection 3(b)(ii) and parametrized from (17) is 0.77. If only *LWP* is used to estimate the rain rate, the correlation falls to 0.60, suggesting that there is some

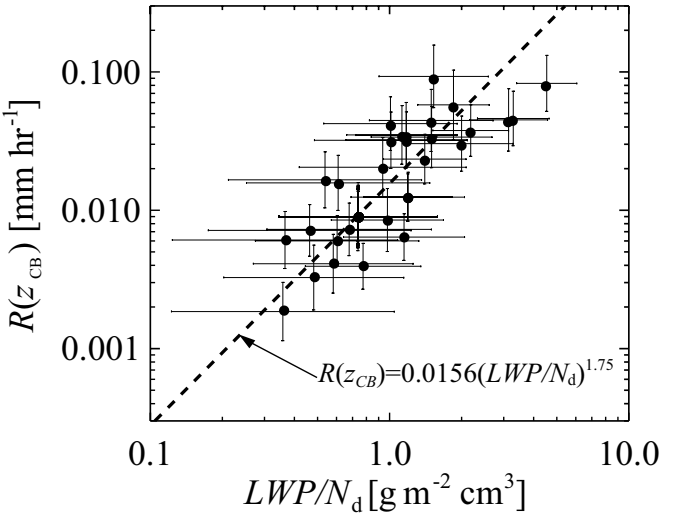

Figure 10. Three-hourly mean cloud-base rain rate, $R(z_{CB})$, derived from the millimetre-wavelength cloud radar, plotted against the ratio of the mean cloud liquid-water path, *LWP*, to the droplet concentration, N_d, with uncertainties. The parametrization described in the text is shown by the dashed line. Uncertainties in *LWP* are assumed to be 25 g m^{-2}, which affects the computation of N_d as well. A conservative estimate of combined uncertainty in rain rate is 60%.

important modulation of the rain rate by changes in droplet concentration (see Fig. 7 in Bretherton *et al.* 2004). However, our data are not sufficient to establish the statistical significance of the R–N_d relationship. Our results are in general qualitative agreement with those of Pawlowska and Brenguier (2003), whose data support a near-quadratic dependence of R_{CB} upon liquid-water path, and an inverse dependence upon cloud droplet concentration. Further observational datasets are necessary to quantify these relationships more accurately.

6. Conclusions

Observations from field campaigns in different Sc regimes were used to obtain relationships between rain rate and radar reflectivity in drizzle for the surface and cloud base. The impact of evaporation below cloud base on Z, R and their relationship was explored with a sedimentation–evaporation model and MMCR reflectivity profiles. Several independent datasets yield an exponent, b, of 1.0–1.1 near the surface and 1.3–1.4 near the cloud base in the relationship $Z = aR^b$ for drizzle. These exponents are lower than the accepted value of 1.5 for deep convective rain. Our suggested Z–R relationship at Sc cloud base is $Z = 25R^{1.3}$.

For exponential or truncated-exponential DSDs, we relate b to the relative variability of N_D and $\overline{r}$ (time series of N_D and $\overline{r}$ are shown in Fig. 5). Variations in rain rate are mainly driven by variations in N_D, while fluctuations in N_D and $\overline{r}$ contribute equally to variations in reflectivity. Understanding the microphysical mechanisms underlying the variability of N_D and $\overline{r}$ will require careful modelling studies and further analyses of aircraft data. The maximum size that a drizzle drop may reach is constrained by the combination of weak updraughts (almost everywhere <1 m s^{-1}) and limited cloud thickness (almost always <500 m). This may have some important consequences for the observation of MBL drizzle from space-borne cloud radar, and deserves additional attention.

Evaporation below cloud base has a significant effect on drizzle DSDs, and therefore Z–R relationships. The coefficient a increases with distance below cloud base, as evaporation of the small drops leads to an increased mean drop size. This makes the derivation of sub-cloud rain rate profiles using only reflectivity difficult. Remote-sensing instruments such as surface-based radar and satellite radar (e.g. CloudSat; Stephens *et al.* 2002) may need to use different Z–R relationships to determine precipitation amounts at various vertical levels where significant changes in the DSD are expected to take place. Bi-level Z–R relationships that were derived for predicting surface rain rate from cloud-base reflectivity show that for low rain rates it is important to account for evaporation below cloud.

Although our radar retrievals of the rainfall amount in the Pacific Sc regions are uncertain to within a factor of three, it is possible to say that area-averaged drizzle rates are highly variable, that sub-cloud evaporation recycles a large fraction of the drizzle before it reaches the surface, and that drizzle is spatially highly inhomogeneous. Areal average drizzle rates frequently exceed 1.0 mm day^{-1} at cloud base, especially in the late night and early morning when Sc is usually thickest. Our best estimate for the EPIC Sc region during 5 days in October 2001 was 0.7 mm day^{-1}, on average, or between 0.2 and 2.3 mm day^{-1} within the range of conservative radar calibration uncertainties. The amount of precipitation reaching the surface is usually significantly less than the amount falling out of the clouds; during EPIC the average was 0.2 mm day^{-1} (ranging from 0.04 to 0.6 mm day^{-1} with uncertainties). Like deep-convective rain, most of the drizzle accumulation comes from a small fraction of the precipitating area.

Drizzle rates in Sc are dependent on both the *LWP* and the cloud droplet concentration, N_{d} (e.g. Austin *et al.* 1995). A linear relationship was found between the derived rain rate and $(LWP/N_{\mathrm{d}})^{1.75}$ during EPIC Sc. The inverse relationship between rain rate and cloud-drop concentration is consistent with previous findings, but more observations are needed to establish the uncertainties in this relationship.

Acknowledgements

The authors wish to thank Christopher Fairall, Taneil Uttal, Duane Hazen, and Paquita Zuidema of NOAA ETL for providing MMCR data and information. We are also grateful to the crew of the NOAA RHB for their assistance in collecting EPIC data, and to the UK Met Office for supplying aircraft DSD data. This research was funded by NSF grant ATM-0082384, NASA grants NAG5S-10624 and NNG04GA65G, and a NDSEG fellowship.

Appendix A

Radar calibration, scan strategy and data processing

(*a*) *MMCR calibration and comparison with C-band data*

After the EPIC cruise, the MMCR was calibrated to within about 1 dBZ (NOAA ETL 2002, 2003, personal communications). Two potential sources of error remain in the MMCR data: Mie scattering and saturation. Drops of radius greater than about 300 μm scatter in the Mie regime, rather than the Rayleigh regime. Figure A.1 shows $Z_{\mathrm{Mie}}/Z_{\mathrm{Rayleigh}}$ as a function of mean radius at the MMCR 8.6 mm wavelength. In Sc drizzle the mean radius of drizzle drops is typically 80 μm or smaller ($<$10% error), calculated from our data. The largest mean drop size obtained by surface filter-paper sampling during EPIC Sc was about 350 μm radius (this is likely to be an overestimate because the detection threshold was 200 μm), so the errors will be at most +20% or

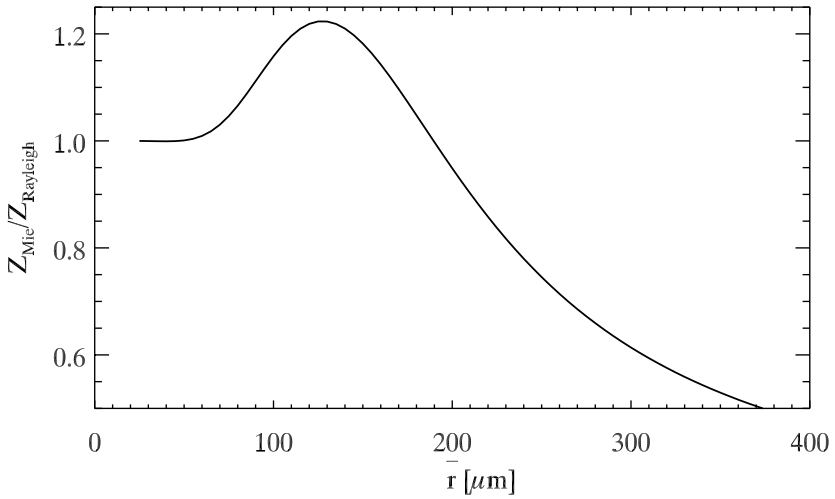

Figure A.1. Ratio between Mie-scattering reflectivity and Rayleigh-scattering reflectivity for drop-size distributions with a mean radius of 0–400 μm.

−50% of the MMCR reflectivity. The larger mean sizes mostly occur well below cloud, when the small drops have evaporated. No MMCR data are used below 400 m, so errors are expected to be smaller than the range stated above. These errors will only occur when the drizzle rate is significant, and we expect them to account for a small fraction of the total error in cloud-base rain rate derived from the MMCR.

The reflectivity value at which the MMCR saturates increases with increasing height (i.e. range). Saturation is about 17 dBZ at mean cloud base and 20 dBZ near mean cloud top (D. Hazen 2003, personal communication). Hourly averaged cloud-base MMCR reflectivity is plotted with hourly area-averaged reflectivity from the C-band radar (discussed in the following sections) in Fig. A.2(a). The C-band reflectivity data in this plot is 'thresholded' at 17 dBZ. Because their time and space resolutions differ, the comparison between the two instruments cannot be exact; however, the two time series track each other fairly well.

Figure A.2(b) shows the ratio of non-thresholded to thresholded hourly area-averaged C-band reflectivity. The curve signifies the reflectivity peaks that the MMCR may be underestimating. Comparison between the MMCR maximum reflectivity data and the thresholded C-band data yields a consistent result, that indicates a relative calibration offset between the C-band and MMCR that is small and positive (i.e. the C-band reflectivity is greater than that from the MMCR).

(*b*) *C-band calibration, scan strategy and quality control*

We estimate that the C-band absolute calibration is within ±2.5 dBZ. In addition to the above comparison that shows C-band data are consistent with the MMCR, two other independent comparisons were performed with radar data from the first leg of the EPIC cruise immediately prior to EPIC Sc. Radar data were compared to TRMM precipitation radar data, and no apparent biases were found (Petersen *et al.* 2003). Mapes and Lin (2005) estimated divergence profiles from the C-band radar data, using several assumptions to compute moisture convergence. Using different Z–R relationships, they found that the calibration offset was likely to be in the range 2.0 to 2.7 dBZ. Our estimation of ±2.5 dBZ is consistent with this result.

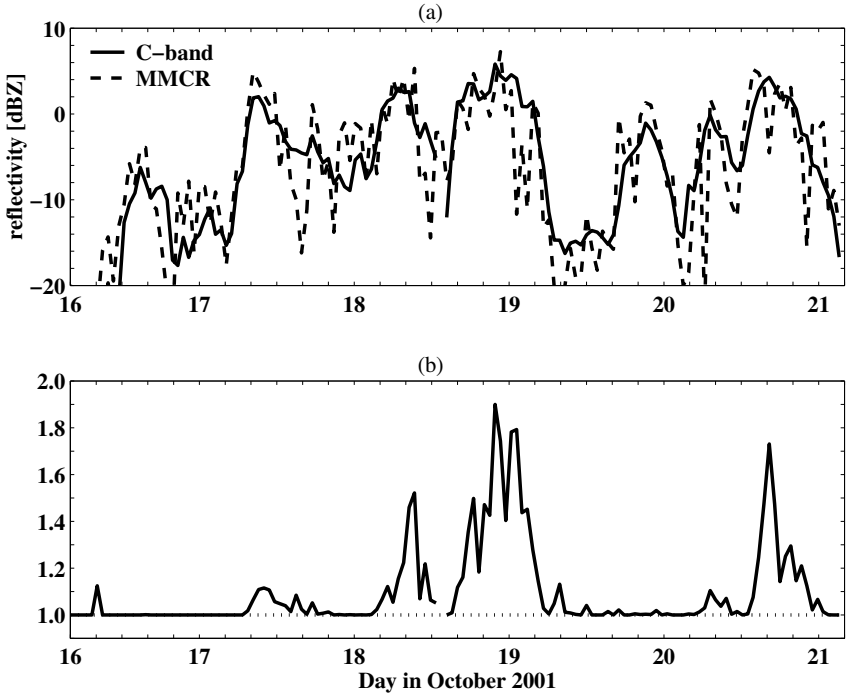

Figure A.2. (a) Time series of hourly-averaged millimetre-wavelength radar (MMCR) cloud-base reflectivity (dashed), and hourly area-averaged C-band radar reflectivity (solid). A threshold of 17 dBZ was imposed on the C-band reflectivity (shown here: C-band $\leqslant$ 17 dBZ). (b) Time series of the ratio of C-band actual hourly area-averaged reflectivity (Z) to C-band thresholded reflectivity. Time is UTC. See text for details.

The C-band radar scan strategy for EPIC Sc was designed to obtain high-resolution temporal and spatial data of the mesoscale structure of drizzling Sc. Constraints on the radar sampling were: the small size of the features of interest, a cloud-top height less than 1.5 km, and a radar echo depth of 500–1000 m. These constraints, combined with the 0.95° beam width of the C-band radar antenna, limited volumetric observations of research quality to within 50 km radius of the ship, and the minimum usable elevation angle to 1°. Due to erroneous values in the signal-processing software, the maximum range of the volume and RHI scans was reduced to 30 km. The centrepiece of EPIC Sc C-band scan strategy was an 11 elevation-angle volume scan every 5 minutes. Volume scans were interspersed with vertical cross-sections six times an hour, and long-range surveillance scans every 30 minutes.

Over 3100 radar volume scans were obtained during EPIC Sc. An automated quality-control algorithm originally developed for TEPPS was fine-tuned to remove questionable echoes in the recorded reflectivity data.

(*c*) *C-band antenna stabilization and interpolation of data to a 2-D grid*

Scanning radar observations from a ship requires antenna stabilization to maintain the antenna pointing angle at the requested elevation with respect to the horizon independent of the motion of the ship. On the RHB, a Seapath Inertial Navigation Unit provides the SIGMET Inc RCP02 antenna controller with information to perform the antenna stabilization and to remove the ship motion from the recorded radial velocity data.

There is usually a $<0.4°$ discrepancy between the requested angle and the antenna pointing angle. There were some concerns about potentially larger pointing-angle errors during EPIC Sc impacting the interpolated reflectivity maps; consequently, for the purposes of this paper, the reflectivity values were averaged between 0.5 and 2 km to yield a 2-D dataset that circumvents this issue.

The 3-D polar coordinate volume scan data were interpolated to a 2-D Cartesian horizontal grid utilizing the National Center for Atmospheric Research Atmospheric Technology Division's REORDER software with Cressman (1959) interpolation. REORDER uses the beam by beam recorded pointing angle, and is well suited to data obtained from moving platforms. The interpolated Cartesian grid has 500 m spacing in the horizontal and extends to 60 km diameter. The weight (W) of a particular radar range gate in deriving the grid point is calculated as follows (Oye and Case 1992):

$$W = \frac{L^2 - l^2}{L^2 + l^2}, \tag{A.1}$$

where l is the distance between the centre of the polar coordinate gate and the centre of the Cartesian grid point, and L is the radius of influence:

$$L^2 = \mathrm{d}X^2 + \mathrm{d}Y^2 + \mathrm{d}Z^2, \tag{A.2}$$

where $\mathrm{d}X$, $\mathrm{d}Y$, and $\mathrm{d}Z$ were set to be a function of range from the radar, a delta azimuth of 0.6°, and a delta elevation of 1.5°. Data below 500 m altitude are not used in the interpolation due to potential sea clutter contamination. The interpolation weights (A.1) peak at 500 m altitude and decrease with increasing altitude.

Appendix B
Statistics for Z–R relationships

Table B.1 compares Z–R relationships of the form $Z = aR^b$ derived from different stratocumulus datasets. Cloud-base and surface Z–R relationships will differ, partly due to differences in data sources. For example, considerable sampling limitations for aircraft data result in poor sampling of the largest drops. These are estimated using exponential extrapolation, as discussed in section 2(b). The primary effect of this in the Z–R relation is a smaller exponent b, shown in Table B.1.

Appendix C
Sedimentation–evaporation model

(a) Model formulation

For a drizzle drop larger than about 20 μm radius, the evaporation rate below cloud base is linearly proportional to the degree of subsaturation and inversely proportional to its radius (Pruppacher and Klett 1997). The constant of proportionality is a fairly weak function of temperature, T, and pressure, p, and it is assumed to be constant for the conditions of this study ($T = 286$ K, $p = 900$ hPa). We model profiles of the size distribution $N(r, z)$ of a population of sedimenting, evaporating drops via the equilibrium relationship:

$$\omega_{\mathrm{T}}(r)\frac{\partial N(r, z)}{\partial z} = -\frac{\partial}{\partial r}\left(N(r, z)\frac{\mathrm{D}r}{\mathrm{D}t}\right), \tag{C.1}$$

TABLE B.1. STATISTICS FOR Z–R RELATIONSHIPS OF THE FORM $Z = aR^b$

1		EPIC filter-paper (surface)	Aircraft (cloud)	Aircraft, no extrapolation	MMCR (cloud base)
2	Best exponent, b	1.1	1.4	1.1	1.3
3	Mean a	57	32	22	25
4	$p_{16\text{th}}$ a	38	17	18	11
5	$p_{84\text{th}}$ a	86	61	28	54
6	Cumulative bias	1.06	0.99	1.12	0.83
7	Average bias	1.07	1.12	1.03	1.17

Rows in the table represent:

1. Datasets used. The columns here are: EPIC (Eastern Pacific Investigation of Climate 2001) Sc filter-paper; UK Met Office aircraft in cloud; Aircraft without using exponential extrapolation to estimate large drop concentrations; cloud-base parameters derived from MMCR (millimetre-wavelength cloud radar).
2. The best exponent, b, from linear least-squares regression, rounded to the nearest tenth.
3. Mean value of a from least-squares regression.
4. 16th percentile value of a from $10^{\{\log a - \text{stdev}(\log a)\}}$.
5. 84th percentile value of a from $10^{\{\log a - \text{stdev}(\log a)\}}$.
6. Cumulative bias for all drop size distribution (DSD) samples in the dataset: $\sum R_{\text{est}} / \sum R_{\text{calc}}$, where R_{est} is estimated from the Z–R relationship, and R_{calc} is calculated from the DSD for each sample.
7. Average bias: $(1/N) \sum (R_{\text{est}}/R_{\text{calc}})$, where N is the total number of DSD samples in the dataset (for further discussion see Hagen and Yuter 2003).

where $\omega_{\text{T}}(r)$ is the terminal velocity of a drop of radius r (e.g. Hall 1980, his Eq. (29), retaining only evaporation/condensation and vertical advection terms, with no time dependence). We use an exponential distribution, truncated at a lower radius of $r_0 = 20$ μm in (3), as the cloud-base boundary condition. Leg- and level-averaged droplet-size distributions in Sc are described well by an exponential distribution (Wood 2005).

We assume that RH is unity at cloud base and decreases linearly below cloud base with a rate 0.36 km^{-1}, the median gradient from rawinsonde profiles during EPIC Sc. Deviations from this RH profile will alter evaporation rates, necessitating different values of k in (4), as illustrated in Fig. C.1. One standard-deviation values of $\text{d}RH/\text{d}z$ are 0.26 and 0.46 km^{-1}; these lead to a RMS fractional error in R_{CB} of only 11% at any one time. We did not find a strong correlation between drizzle and the value of $\text{d}RH/\text{d}z$, so errors in R_{CB} will tend not to be correlated with R_{CB}. Because the Z–R relationship is nearly linear, introducing a random uncorrelated error in $\text{d}RH/\text{d}z$ leads to only small changes in the Z–R relationship.

We use a single power-law terminal-velocity relationship in the model (see (6)). Ventilation coefficients are taken from Pruppacher and Klett (1997) and increase almost linearly from approximately unity at $r = 20$ μm to 5.2 at $r = 500$ μm. Finally, we assume that the drops are falling below cloud in still air, i.e. there are no turbulent motions. Turbulent motions *are* responsible for the growth and development of the drizzle DSD within cloud (Nicholls 1987; Baker 1993; Austin *et al.* 1995). No direct observational evidence exists to show how the sizes and concentrations of drizzle drops are correlated with vertical wind fluctuations in the cloud-base and sub-cloud regions. There may be considerable errors associated with the still-air assumption. This is addressed below in subsection (b), but requires more investigation, both in observations and models.

We calculate $N(r, z)$ numerically, by solving (C.1) as a function of height below cloud for the temperature range 270–290 K and for cloud-base mean radius $\overline{r}$ from 30–80 μm, which covers the range of MMCR observations. We then calculate the

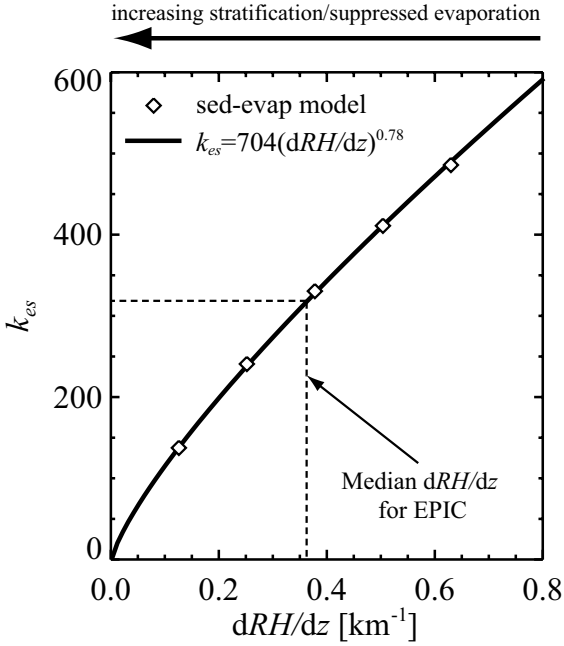

Figure C.1. Values of k in (4) (given as $k_{\rm es}$ in figure) as a function of relative-humidity gradient below cloud (d*RH*/dz). The median *RH* gradient for EPIC corresponds to $k = 320\ \mu\text{m}^{3.75}\text{m}^{-1.5}$. The curve represents a fit to results from the sedimentation–evaporation model (diamonds) for different *RH* gradients. See text for details.

precipitation rate normalized with its cloud-base value as a function of distance below cloud base. The rate of decrease in rain rate with height is lower when the mean radius is larger, because larger drops fall faster and evaporate more slowly. A good parametrization of the model results is provided in (4).

Results from the sedimentation–evaporation model are presented in Fig. C.2, which shows normalized profiles of rain rate $R/R_{\rm CB}$ against the height parameter $\chi = \{(z_{\rm CB} - z)/(\overline{r})^{2.5}\}^{1.5}$ that best collapses the different model conditions. The parametrization of (4) is also shown, and clearly represents a good fit to the model results over the range of cloud-base mean radii typical in drizzling Sc clouds. Figure C.2(b) shows the relationship between $R/R_{\rm CB}$ and $Z/Z_{\rm CB}$ together with the parametrization expressed in (5).

(b) Sources of error and considerations

The spread in observational values is a result of two main factors: (i) there is considerable spatial variability in the cloud-base height; (ii) turbulent mixing in the cloud–sub-cloud layer can alter the drizzle drop profiles. The latter was also noted by Nicholls (1987) who compared sub-cloud DSDs with the results of a numerical model. Nicholls' model assumes still air beneath cloud base, and results in drop concentrations decreasing faster with height below base than those measured. However, we find that the simple sedimentation–evaporation model can reproduce fairly well the observed decrease in precipitation rate below cloud base.

Vali *et al.* (1998) present the only observations published to date of correlations between radar reflectivity and vertical wind from three cases of marine stratus/Sc. In the sub-cloud region these correlations are of the order -0.25. The correlations are negative because in the sub-cloud layer there is a positive gradient of reflectivity with

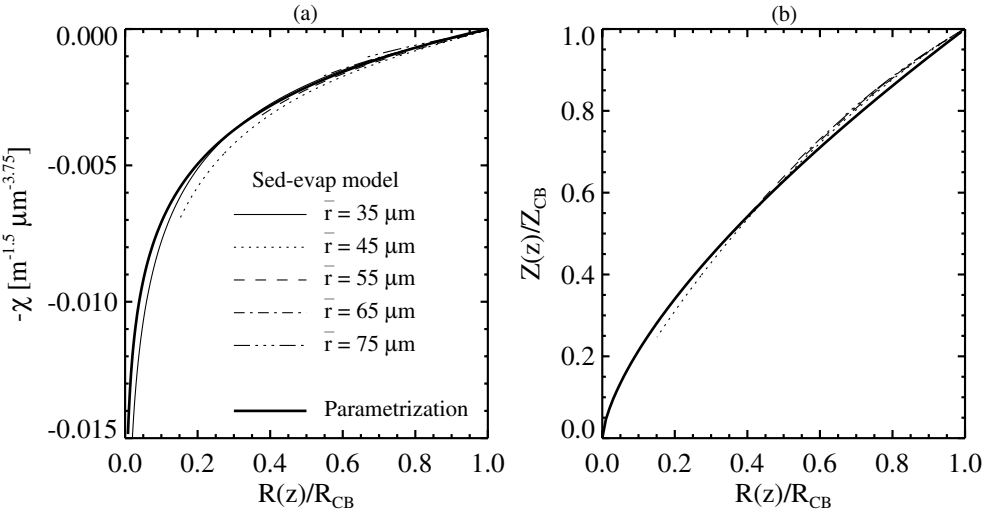

Figure C.2. Results from the sedimentation–evaporation model: (a) profiles of normalized rain rate R/R_{CB} against the normalized height parameter χ from the model (thin lines), together with the analytical parametrization (thick solid line) in (4); (b) R/R_{CB} plotted against normalized radar reflectivity Z/Z_{CB} from the model (thin lines) together with the analytical parametrization (thick solid line). The key in (a) also applies to (b) but similarities are such that many lines are effectively superimposed. See text for details.

height and a downward turbulent transport of drizzle drops from the more reflective cloud layer. The correlations result in profiles of R that decrease less rapidly with height (for a given ensemble mean $\overline{r}$) than profiles with no correlation. Therefore, using a still-air value of k (see (4)) to derive $\overline{r}$ results in an overestimate if negative correlations between reflectivity and vertical wind are neglected. We simulate the effect of such a negative correlation between reflectivity and vertical wind using an ensemble of 100 realizations of the sedimentation–evaporation model with a range of updraughts and downdraughts. A constant vertical-wind standard deviation $\sigma_{\mathrm{w}} = 0.6\ \mathrm{m\ s^{-1}}$ is used, which is representative of turbulence in relatively deep cloud-topped MBLs. Observations from the MMCR suggest that in time-scales less than an hour, the standard deviation of the radar reflectivity is approximately 5–10 dBZ. The model size distributions are initialized to give an ensemble of parcels with these statistical properties. We also assume that the updraughts/downdraughts are coherent through the depth of the sub-cloud layer. Using these ensembles, the approximate overestimate of $\overline{r}$ depends upon the magnitude of $\overline{r}$, decreasing as $\overline{r}$ increases, with errors of 30, 15 and 5% for $\overline{r} = 40$, 55 and 75 μm, respectively. These overestimates in $\overline{r}$ propagate to overestimates in R_{CB} of 67, 35 and 12%, respectively, and corresponding underestimates of R_{sfc} of a similar magnitude. These errors, while non-negligible, are somewhat lower than the uncertainties associated with the C-band calibration (see appendix A).

APPENDIX D
DERIVATION OF AN EXPRESSION FOR b

We define $u = \log N_{\mathrm{D}}$ and $v = \log \overline{r}$ to be normally distributed with standard deviations $\sigma_u = \log N_{\mathrm{D}}$ and $\sigma_v = \sigma_{\log \overline{r}}$, respectively. We wish to find the least-squares optimal value of the exponent b in the relationship $Z_{\mathrm{CB}} = aR_{\mathrm{CB}}^b$, where $\log(Z_{\mathrm{CB}}) = u + \beta_1 v$ and $\log(R_{\mathrm{CB}}) = u + \beta_2 v$, from (14) and (15). Taking the logarithm of the Z–R relationship with $\log(Z_{\mathrm{CB}})$ as the independent variable as in (2), the optimal value of b

is given by (e.g. Press *et al.* 1992):

$$
\begin{aligned}
b &= \frac{1}{\mathrm{r}_{\log Z \log R}} \frac{\sigma_{\log Z}}{\sigma_{\log R}} \\
&= \frac{1}{\mathrm{r}_{\log Z \log R}} \frac{\sigma_{(u+\beta_1 v)}}{\sigma_{(u+\beta_2 v)}} \\
&= \frac{1}{\mathrm{r}_{\log Z \log R}} \left\{ \frac{\sigma_u^2 + \beta_1^2 \sigma_v^2 + 2\beta_1 \sigma_u \sigma_v \mathrm{r}_{\log N_\mathrm{D} \log \overline{r}}}{\sigma_u^2 + \beta_2^2 \sigma_v^2 + 2\beta_2 \sigma_u \sigma_v \mathrm{r}_{\log N_\mathrm{D} \log \overline{r}}} \right\}^{\frac{1}{2}},
\end{aligned}
$$

which results in the expression given in (16).

References

Austin, P., Wang, Y., Pincus, R. and Kujala, V. 1995 Precipitation in stratocumulus clouds: Observations and modeling results. *J. Atmos. Sci*., **52,** 2329–2352

Baker, M. B. 1993 Variability in concentrations of cloud condensation nuclei in the marine cloud-topped boundary layer. *Tellus*, **45B,** 458–472

Bower, K. N., Choularton, T. W., Baker, M. B., Blyth, A., Nelson, J. and Jensen, J. 1992 'Microphysics of warm clouds; measurements and discussion'. P. 133 in Proceedings of the 11th international conference on clouds and precipitation, Montreal, Canada. International Association of Meteorology and Atmospheric Physics. Toronto, Canada

Bretherton, C. S., Austin, P. and Siems, S. T. 1995 Cloudiness and marine boundary layer dynamics in the ASTEX Lagrangian experiments. Part II: Cloudiness, drizzle, surface fluxes, and entrainment. *J. Atmos. Sci*., **52,** 2724–2735

Bretherton, C. S., Uttal, T., Fairall, C. W., Yuter, S. E., Weller, R. A., Baumgardner, D., Comstock, K. and Wood, R. 2004 The EPIC 2001 stratocumulus study. *Bull. Am. Meteorol. Soc.*, **85,** 967–977

Campos, E. and Zawadzki, I. 2000 Instrumental uncertainties in Z–R relations. *J. Appl. Meteorol.*, **39,** 1088–1102

Cressman, G. P. 1959 An operational objective analysis system. *Mon. Weather Rev.*, **87,** 367–374

Doelling, I. G., Joss, J. and Riedl, J. 1998 Systematic variations of Z–R relationships from drop size distributions measured in northern Germany during seven years. *Atmos. Res*., **47–48,** 635–649

Dong, X. and Mace, G. G. 2003 Arctic stratus cloud properties and radiative forcing derived from ground-based data collected at Barrow, Alaska. *J. Climate*, **16,** 445–460

Fairall, C. W., Hare, J. E. and Snider, J. B. 1990 An eight-month sample of marine stratocumulus cloud fraction, albedo, and integrated liquid water. *J. Climate*, **3,** 847–864

Gunn, R. and Kinzer, G. D. 1949 The terminal velocity of fall for water droplets in stagnant air. *J. Meteorol.*, **6,** 243–248

Hagen, M. and Yuter, S. E. 2003 Relations between radar reflectivity, liquid water content, and rainfall rate during the MAP-SOP. *Q. J. R. Meteorol. Soc*., **129,** 477–493

Hall, W. 1980 A detailed microphysical model within a two-dimensional dynamic framework: Model description and preliminary results. *J. Atmos. Sci.*, **37,** 2486–2507

Jensen, J. B., Lee, S., Krummel, P. B., Katzfey, J. and Gogoasa, D. 2000 Precipitation in marine cumulus and stratocumulus. Part I: Thermodynamic and dynamic observations of closed cell circulations and cumulus bands. *Atmos. Res.*, **54,** 117–155

Joss, J. and Gori, E. G. 1978 Shapes of raindrop size distributions. *J. Appl. Meteorol.*, **17,** 1054–1061

Joss, J., Schram, K., Thams, J. C. and Waldvogel, A. 1970 'On the quantitative determination of precipitation by radar'. Scientific Report 63, Eidgenössische Kommission zum Studium der Hagelbildung und der Hagelabwehr. Zurich, Switzerland

Khairoutdinov, M. F. and Kogan, Y. L. 2000 A new cloud physics parametrization in a large-eddy simulation model of marine stratocumulus. *Mon. Weather Rev.*, **128,** 229–243

Klein, S. A. and Hartmann, D. L. 1993 The seasonal cycle of low stratiform clouds. *J. Climate*, **6,** 1587–1606

Li, X. and Srivastava, R. C. 2001 An analytical solution for raindrop evaporation and its application to radar rainfall measurements. *J. Appl. Meteorol.*, **40,** 1607–1616

Mapes, B. E. and Lin, J. 2005 Doppler radar observations of mesoscale wind divergence in regions of tropical convection. *Mon. Weather Rev.*, in press

Marshall, J. S. and Palmer, W. M. 1948 The distribution of raindrops with size. *J. Meteorol.*, **5,** 165–166

Miller, M. A. and Albrecht, B. A. 1995 Surface-based observations of mesoscale cumulus–stratocumulus interaction during ASTEX. *J. Atmos. Sci.*, **52,** 2809–2826

Moran, K. P., Martner, B. E., Post, M. J., Kropfli, R. A., Welsh, D. C. and Widener, K. B. 1998 An unattended cloud-profiling radar for use in climate research. *Bull. Am. Meteorol. Soc.*, **79,** 443–455

Nicholls, S. 1987 A model of drizzle growth in warm, turbulent, stratiform clouds. *Q. J. R. Meteorol. Soc.*, **113,** 1141–1170

O'Connor, E. J., Hogan, R. J. and Illingworth, A. J. 2004 Retrieving stratocumulus drizzle parameters using Doppler radar and lidar. *J. Appl. Meteorol.*, in press

Oye, D. and Case, M. 1992 'REORDER—A program for gridding radar data: Installation and user manual for the UNIX version'. Available from NCAR ATD, Boulder CO, USA

Pawlowska, H. and Brenguier, J.-L. 2003 An observational study of drizzle formation in stratocumulus clouds for general circulation model (GCM) parameterizations. *J. Geophys. Res.*, **108,** 803–821

Petersen, W. A., Cifelli, R., Boccippio, D. J., Rutledge, S. A. and Fairall, C. 2003 Convection and easterly wave structures observed in the eastern Pacific warm pool during EPIC-2001. *J. Atmos. Sci.*, **60,** 1754–1773

Philander, S. G. H., Gu, D., Halpern, D., Lambert, G., Lau, N.-C., Li, T. and Pacanowski, R. C. 1996 Why the ITCZ is mostly north of the equator. *J. Climate*, **9,** 2958–2972

Press, W. H., Teukolsky, S. A., Vetterling, W. T. and Flannery, B. P. 1992 *Numerical recipes in Fortran. The art of scientific computing*. Second edition, Cambridge University Press, Cambridge, UK

Pruppacher, H. R. and Klett, J. D. 1997 *Microphysics of clouds and precipitation*, Second edition, Kluwer Academic Publishers, Dordrecht, the Netherlands

Rinehart, R. E. 1997 *RADAR for meteorologists*. Third edition. Rinehart Publications, Grand Forks, North Dakota, USA

Rogers, R. R. and Yau, M. K. 1989 *A short course in cloud physics*, Third edition. Butterworth–Heinemann, Oxford, UK

Ryan, M., Post, M. J., Martner, B., Novak, J. and Davis, L. 2002 'The NOAA *Ron Brown*'s shipboard Doppler precipitation radar'. In Proceedings of the sixth symposium on integrated observing systems, Orlando, Florida, January 2002. American Meteorological Society, Boston, USA

Slingo, A. 1990 Sensitivity of the earth's radiation budget to changes in low clouds. *Nature*, **343,** 49–51

Smith, P. L. and Joss, J. 1997 'Use of a fixed exponent in 'adjustable' Z–R relationships'. Pp. 254–255 in Preprints of the 28th conference on radar meteorology, Austin, Texas. American Meteorological Society, Boston, USA

Smith, P. L., Liu, Z. and Joss, J. 1993 A study of sampling variability effects in raindrop size observations. *J. Appl. Meteorol.*, **32,** 1259–1269

Steiner, M. and Smith, J. A. 2000 Reflectivity, rain rate, and kinetic energy flux relationships based on raindrop spectra. *J. Appl. Meteorol.*, **39,** 1923–1940

Steiner, M., Smith, J. A. and Uijlenhoet, R. 2004 A microphysical interpretation of the radar reflectivity–rain rate relationship. *J. Atmos. Sci.*, **61,** 1114–1131

Stephens, G. L., Vane, D. G., Boain, R. J., Mace, G. G., Sassen, K., Wang, Z., Illingworth, A. J., O'Connor, E. J., Rossow, W. B., Durden, S. L., Miller, S. D., Austin, R. T., Benedetti, A. and Mitrescu, C. 2002 The CloudSat mission and the A-Train. *Bull. Am. Meteorol. Soc.*, **83,** 1771–1790

Stevens, B., Lenschow, D. H., Vali, G., Gerber, H., Bandy, A., Blomquist, B., Brenguier, J.-L., Bretherton, C. S., Burnet, F., Campos, T., Chai, S., Faloona, I., Friesen, D., Haimov, S., Laursen, K., Lilly, D. K., Loehrer, S. M., Szymon Malinowski, P., Morley, B., Petters, M. D., Rogers, D. C., Russell, L., Savic-Jovcic, V., Snider, J. R., Straub, D., Marcin Szumowski, J., Takagi, H., Thornton, D. C., Tschudi, M., Twohy, C., Wetzel, M. and van Zanten, M. C. 2003 Dynamics and chemistry of marine stratocumulus—DYCOMS II. *Bull. Am. Meteorol. Soc.*, **84,** 579–593

Tripoli, G. J. and Cotton, W. R. 1980 A numerical investigation of several factors contributing to the observed variable intensity of deep convection over south Florida. *J. Appl. Meteorol*., **19,** 1037–1063

Turton, J. D. and Nicholls, S. 1987 A study of the diurnal variation of stratocumulus using a multiple mixed layer model. *Q. J. R. Meteorol. Soc*., **113,** 969–1009

Vali, G., Kelly, R. D., French, J., Haimov, S., Leon, D., McIntosh, R. E. and Pazmany, A. 1998 Finescale structure and microphysics of coastal stratus. *J. Atmos. Sci.*, **55,** 3540–3564

Wood, R. 2005 Drizzle in stratiform boundary layer clouds. Part I: Vertical and horizontal structure. *J. Atmos. Sci.*, in press

Yuter, S. E. and Parker, W. S. 2001 Rainfall measurement on ships revisited: The 1997 PACS TEPPS cruise. *J. Appl. Meteorol.*, **40,** 1003–1018

Yuter, S. E., Serra, Y. L. and Houze, R. A. 2000 The 1997 Pan American climate studies tropical eastern Pacific process study. Part II: Stratocumulus region. *Bull. Am. Meteorol. Soc.*, **81,** 483–490